SGD and Weight Decay Secretly Minimize the Rank of Your Neural Network

Tomer Galanti
Texas A&M University
galanti@tamu.edu

Zachary Siegel
Princeton University
zss@princeton.edu

Aparna Gupte
Massachusetts Institute of Technology
agupte@mit.edu

Tomaso Poggio
Center for Brains, Mind, and Machines
Massachusetts Institute of Technology
tp@csail.mit.edu

Abstract

We investigate the inherent bias of Stochastic Gradient Descent (SGD) toward learning low-rank weight matrices during the training of deep neural networks. Our results demonstrate that training with mini-batch SGD and weight decay induces a bias toward rank minimization in the weight matrices. Specifically, we show both theoretically and empirically that this bias becomes more pronounced with smaller batch sizes, higher learning rates, or stronger weight decay. Additionally, we predict and empirically confirm that weight decay is essential for this bias to occur. Unlike previous literature, our analysis does not rely on assumptions about the data, convergence, or optimality of the weight matrices, making it applicable to a wide range of neural network architectures of any width or depth. Finally, we empirically explore the connection between this bias and generalization, finding that it has a marginal effect on the test performance.

1 Introduction

Stochastic gradient descent (SGD) is one of the most widely used optimization techniques for training deep learning models [1]. While initially developed to mitigate the computational challenges of traditional gradient descent, recent studies suggest that SGD also plays a crucial role in regularization, helping prevent overparameterized models from converging to minima that do not generalize well [2, 3, 4, 5]. Empirical research has shown, for example, that SGD can outperform gradient descent [5], with smaller batch sizes leading to better generalization [6, 4]. However, the full extent of SGD's regularization effects is not yet fully understood.

Various studies have shown that when training large neural networks using gradient-based optimization, the networks tend to become highly compressible. For example, many papers have demonstrated that a significant portion of the weights can be pruned post-training [7, 8, 9, 10, 11, 12], large pre-trained models can be distilled into smaller models [13, 14, 15, 16], and in some cases, the learned weight matrices can be approximated using low-rank matrices without a significant loss in accuracy [17, 18, 19, 20, 21, 22].

While these empirical observations provide promising evidence that neural networks can be compressed in various ways, controlling the compression requires theoretical guidance to understand how it is influenced by different aspects of the learning process, such as hyperparameters, data, and model architecture. To address this gap, several attempts have been made to explore the origins of the low-rank bias. For instance, in [23, 24, 25], researchers examined the rank of weight matrices

Preprint. Under review.

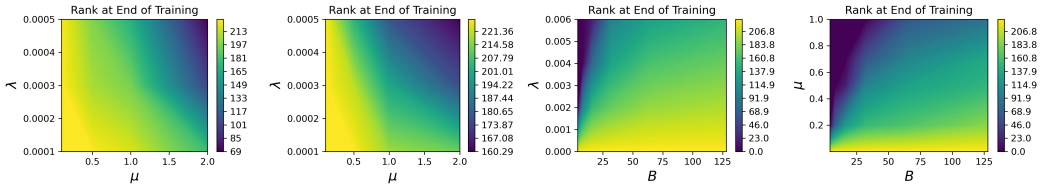

(a) $B = 8$ **(b)** $B = 16$ **(c)** $\mu = 0.5$ **(d)** $\lambda = 6e - 3$

Figure 1: **Higher weight decay (λ) and learning rate (μ), or smaller batch sizes (B), lead to a lower average rank across the network layers.** We plot the average rank at end of training for ResNet-18 trained on CIFAR10 when varying a pair of hyperparameters.

Table 1: **The assumptions and results of various papers on low-rank bias in deep learning.** The last column shows the result of each paper. The notation Lin_L denotes a composition of L linear layers, and σ represents the ReLU activation. N/A is used when the paper does not specify a constraint. Our paper considers a much more realistic setting than all of the previous papers.

Paper	Architecture	Data	Objective function	Optimizer	Convergence	Result
[26]	Lin_L	Linearly separable	Exponential/logistic loss	GF	N/A	Each layer has rank ≤ 1
[28]	$\text{Lin}_1 \circ \sigma \circ \text{Lin}_1$	1-dimensional	Min L_2 regularization s.t. data fitting	N/A	Global optimum	First layer has rank ≤ 1
[24]	$\text{Lin}_1 \circ \sigma \circ \text{Lin}_L$	d-dimensional	Min L_2 regularization s.t. data fitting	N/A	Global optimum	Bottom linear transformation has rank $\leq d$
[27]	$\text{Lin}_K \circ \sigma \circ \text{Lin}_1 \circ \ldots \sigma \circ \text{Lin}_1$	Linearly separable	Exponential/logistic loss	GF	N/A	Top K layers have rank ≤ 1
[25]	$\text{Lin}_1 \circ \sigma \circ \text{Lin}_1 \circ \ldots \sigma \circ \text{Lin}_1$	Separable by a depth L' network	Min L_2 regularization s.t. fitting the data	N/A	Global optimum	Top $L - L'$ layers have rank ≤ 2
Ours	Res, Conv, Lin, Activation	N/A	Differentiable loss + L_2 regularization	SGD	N/A	Each layer has rank $\mathcal{O}(1)$ (w.r.t the width)

in neural networks that globally minimize L_2 regularization while fitting the training data. Specifically, [23] demonstrated that for data on a 1-dimensional manifold, the weight matrices of a two-layer network become rank-1 at the global minimum. This result was later extended in [24], showing that the weight matrix has rank $\leq d$ when the data lies in a d-dimensional space. Additionally, [25] found that in sufficiently deep ReLU networks, the weight matrices at the top-most layers become low-rank at the global minimum. Similarly, [26] showed that gradient flow (GF) training of univariate linear networks with exponentially-tailed classification losses learns rank-1 weight matrices when the data is linearly separable. A more recent study [27] extended this result, demonstrating that when training a ReLU network with multiple linear layers at the top using GF, the top layers converge to rank-1 weight matrices.

While these analyses offer valuable insights, each one makes strong assumptions about the structure of the data (e.g., linear separability, low-dimensionality), the network architecture, the optimization method, or the objective function, and they only apply to specific layers of the network. Moreover, these analyses reveal little about the relationship between the low-rank bias and the training hyperparameters or the model architecture, which limits the practical utility of these results.

Contributions. In this paper, we show that using mini-batch Stochastic Gradient Descent (SGD) and weight decay ***implicitly minimizes the rank*** of the learned weight matrices during the training of neural networks, particularly encouraging the ***learning of low-dimensional feature manifolds***. Within the active field that investigates these properties [29, 26, 28, 27, 25], our analysis is the first to characterize how SGD and weight decay induce a low-rank bias in all of the weight matrices of a wide range of neural network architectures (e.g., with residual connections [30], self-attention layers [31] and convolutional layers [32]), without making assumptions about the data (e.g., linear separability or low-dimensionality) or strong assumptions about the convergence of the training process. Our theoretical analysis predicts that smaller batch sizes, higher learning rates, or increased weight decay results in a decrease in the rank of the learned matrices, and that weight decay is necessary to achieve this bias. Our results are compared with the previous literature in Tab. 1.

To validate our theory, we provide a comprehensive empirical analysis in which we examine the regularization effects of different hyperparameters on the rank of weight matrices for various network architectures. Additionally, we carried out several experiments to examine the connection between low-rank bias and generalization. Our findings suggest that although low-rank bias is not crucial for good generalization, it is correlated with a slight improvement in performance.

2 Problem Setup

We study the influence of using mini-batch SGD in conjunction with weight decay on the ranks of the learned weight matrices of neural networks in standard learning settings. Namely, we consider a parametric model $\mathcal{F} \subset \{f' : \mathcal{X} \to \mathbb{R}^q\}$, where each function $f_W \in \mathcal{F}$ is specified by a vector of parameters $W \in \mathbb{R}^N$. The goal is to learn a function from a training dataset $S = \{x_i\}_{i=1}^m$. For each sample we have a loss function measuring the performance on that sample $\ell_i : \mathbb{R}^q \to \mathbb{R}$ which is simply a differentiable function. For example, in supervised learning we have $\ell_i(u, y_i)$, where y_i is the label of the ith sample. The model is trained to minimize the regularized empirical risk,

$$L_S^\lambda(f_W) \ := \ \frac{1}{m}\sum_{i=1}^{m} \ell_i(f_W(x_i)) + \lambda\|W\|_2^2, \tag{1}$$

where $\lambda > 0$ is a predefined hyperparameter and $\|\cdot\|_2$ is the Frobenius norm. To accomplish this task, we typically use mini-batch SGD, as outlined in the following paragraph.

Model architecture. In this paper, we consider a broad set of neural network architectures, including but not limited to neural networks with fully-connected layers, residual connections, convolutional layers, pooling layers, sub-differentiable activation functions (e.g., sigmoid, tanh, ReLU, Leaky ReLU), self-attention layers and siamese layers.

In this framework, the model $f_W(x) := h(x; W^1, \ldots, W^k)$ is a function that takes a sequence of weight matrices $W^1, \ldots, W^k$ and an input vector x. Throughout the paper, we assume that for each layer $l \in [k]$, we can write

$$f_W(x) = g_l(W^l u_1^l(x, W_{|l}), \ldots, W^l u_{m_l}^l(x, W_{|l}), W_{|l}, x), \tag{2}$$

where g_l is a sub-differentiable function accepting vectors $W^l u_j^l(x, W_{|l})$, the parameters $W_{|l} = \{W^j\}_{j\neq l}$ and x as input. Here, $u_j^l(x, W_{|l})$ are functions of x and the weight matrices $W_{|l}$, viewed as a layer preceding W^l.

For example, a neural network with a fully-connected layer can be written as follows:

$$f_W(x) = g_l(W^l u^l(x, W_{|l}), W_{|l}, x), \tag{3}$$

where $u^l(x, W_{|l})$ is the input to the fully-connected layer and $g_l(z, W_{|l}, x)$ takes the output $z = W^l u^l(x, W_{|l})$ of the fully-connected layer and returns the output of the neural network (e.g., by composing multiple layers on top of it). More specifically, a fully-connected network $f_W(x) = W^L\sigma(W^{L-1}\cdots W^2\sigma(W^1 x)\cdots)$ can be written as $g_l(W^l u^l(x, W_{|l}))$, where $g_l(z) = W^L\sigma(W^{L-1}\cdots W^{l+1}\sigma(z)\cdots)$ and $u^l(x, W_{|l}) = \sigma(W^{l-1}\cdots W^2\sigma(W^1 x)\cdots)$. We can also represent convolutional layers within this framework. We can think of a convolutional layer as a transformation that takes some input u and applies the same linear transformation to multiple 'patches' independently, $W^l u_1^l, \ldots, W^l u_{m_l}^l$, where each u_j^l denotes a patch in the input u (a patch in this case is a subset of the coordinates in u), m_l is the number of patches and $W^l \in \mathbb{R}^{c_l \times c_{l-1} d_{l-1}}$ is a matrix representation of the kernel. In this case, $u^l(x, W_{|l})$ is the output of the layer below the convolutional layer and $u_j^l(x, W_{|l})$ is the jth patch that the convolutional layer is applied to. Furthermore, g_l is simple the composition of the layers following the given convolutional layer. In similar ways, we can also express neural networks with residual connections, self-attention layers, hypernetwork layers, pooling layers, etc'.

Optimization. We employ stochastic sub-gradient descent (SGD) to minimize the regularized empirical risk $L_S^\lambda(f_W)$ over a specified number of iterations T. We begin by initializing W_1 at some point. We split the data S into $r = \frac{|S|}{B}$ batches of size B (for simplicity we assume that $|S|$ is divisible by B) and at iteration t, we take batch $\tilde{S}_{t'}$ with $t' = (t \mod r)$ and update $W_{t+1} = W_t - \mu\nabla_W L_{\tilde{S}_{t'}}^\lambda(f_{W_t})$, where $\mu > 0$ is the predefined learning rate and $\nabla_W g(W)$ represents a sub-gradient of $g : \mathbb{R}^n \to \mathbb{R}$. We use sub-gradient descent when dealing with models that are only sub-differentiable, such as ReLU neural networks (for more details, see section 14.2 in [33]). It is worth noting that when the model is differentiable, sub-gradient descent aligns with gradient descent.

3 Theoretical Results

In this section, we prove that when training neural networks with regularized SGD for a long time, the weight matrices can be approximated with matrices of bounded ranks. We begin by making a simple observation that the rank of $\nabla_{W^l}\ell(f_W(x))$ is bounded by m_l (see 'Model architecture' in Sec. 2) for any l and any sample x. Then, by recursively unrolling the optimization process, we express the weight matrix W_T^l as a sum of $(1-\mu\lambda)^n W_{T-n}^l$ and nB gradients of the loss function with respect to W^l for different samples at different iterations. Since each one of these terms is a matrix of rank $\leq m_l$, we conclude that the distance between W_T^l and a matrix of rank $\leq m_l Bn$ decays exponentially fast when increasing n.

Lemma 3.1. *Let ℓ be a differentiable loss function, and let f_W be a model as described in Sec. 2. For any weight matrix W^l in f_W and any sample $x \in \mathbb{R}^d$, the following inequality holds:*

$$\text{rank}\left(\nabla_{W^l}\ell(f_W(x))\right) \;\leq\; m_l,$$

where m_l is a constant depending on the structure of the layer l (defined in Eq. 2).

The above lemma shows the rank of the gradient with respect to any weight matrix W^l is bounded by $\leq m_l$. In particular, for a fully-connected layer with weight matrix W^l, the sub-gradient of the loss function with respect to W^l is at most 1 and for a convolutional layer it is bounded by the number of patches upon which the kernel is being applied.

The following lemma provides an upper bound on the minimal distance between the network's weight matrices and matrices of bounded rank.

Lemma 3.2. *Let $\|\cdot\|$ be any matrix norm and ℓ any differentiable loss function. Consider a model f_W as described in Sec. 2 and W^l be a weight matrix within f_W. Suppose we train f_W using SGD with batch size $B \in [m]$, learning rate $\mu > 0$ and weight decay $\lambda > 0$, where m is the total number of training samples. Then, for any integer $T > n$, the following inequality holds:*

$$\min_{\bar{W}^l:\ \text{rank}(\bar{W}^l)\leq m_l Bn} \left\| \frac{W_T^l}{\|W_T^l\|} - \bar{W}^l \right\| \;\leq\; (1-2\mu\lambda)^n \cdot \frac{\|W_{T-n}^l\|}{\|W_T^l\|}.$$

The lemma above provides an upper bound on the minimal distance between the parameters matrix W_T^{ij} and a matrix of rank $\leq m_l Bn$. The parameter t is a parameter of our choice that controls the looseness of the bound and is independent of the optimization process. The bound is proportional to $(1-2\mu\lambda)^n \frac{\|W_{T-n}^l\|}{\|W_T^{ij}\|}$, which decreases exponentially with n as long as $\|W_T^l\|$ converges to a non-zero value. As a next step, we tune t to ensure that the bound would be smaller than ϵ. This result is summarized in the next theorem.

Theorem 3.3. *Let $\|\cdot\|$ be any matrix norm and ℓ a differentiable loss function and $\mu, \lambda > 0$ such that $\mu\lambda < 0.5$, $B \in [m]$, and $\epsilon > 0$. Consider a model f_W as described in Sec. 2 and W^l be a weight matrix within f_W. Suppose we train f_W using SGD with batch size $B \in [m]$, learning rate $\mu > 0$ and weight decay $\lambda > 0$, where m is the total number of training samples. Assume that $\lim_{T\to\infty}(\|W_{T-1}^l\|/\|W_T^l\|) = 1$. Then, for sufficiently large T,*

$$\min_{\bar{W}^i:\ \text{rank}(\bar{W}^i)\leq \frac{m_l B\log(2/\epsilon)}{2\mu\lambda}} \left\| \frac{W_T^l}{\|W_T^l\|} - \bar{W}^i \right\| \;\leq\; \epsilon.$$

The above theorem provides an upper bound on the rank of the learned weight matrices. It shows that when training the model, the normalized weight matrices $\frac{W_T^l}{\|W_T^l\|}$ become approximately matrices of rank at most $\frac{m_l B\log(2/\epsilon)}{2\mu\lambda}$. While $\frac{m_l B\log(2/\epsilon)}{2\mu\lambda}$ is not necessarily a small number, this bound is still non-trivial since $\frac{m_l B\log(2/\epsilon)}{2\mu\lambda} = \mathcal{O}(1)$ with respect to the iteration t and the size of the network (its width,

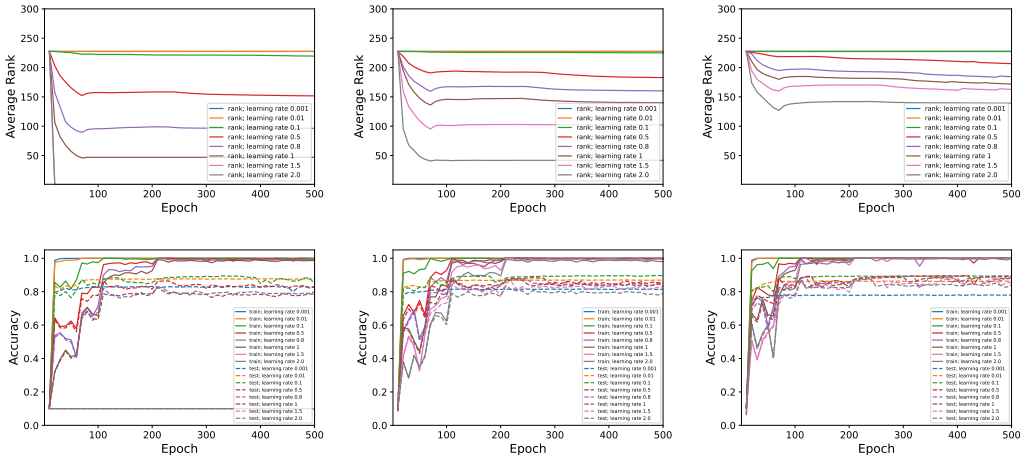

$B = 4$ $B = 8$ $B = 16$

Figure 2: **Average ranks and accuracy rates of ResNet-18 trained on CIFAR10 when varying μ.** The top row shows the average rank across layers, while the bottom row shows the train and test accuracy rates for each setting. In this experiment, $\lambda = 5\text{e}{-4}$ and $\epsilon = 1\text{e}{-3}$.

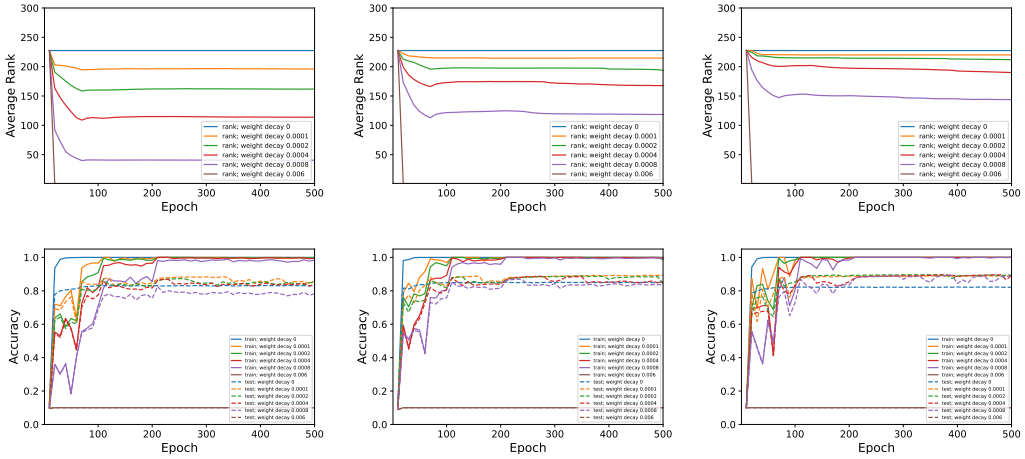

$B = 8$ $B = 16$ $B = 32$

Figure 3: **Average ranks and accuracy rates of ResNet-18 trained on CIFAR10 when varying λ.** In this experiment, $\mu = 1.5$ and $\epsilon = 1\text{e}{-3}$.

depth, etc'). This result is particularly striking as it reveals a mechanism that encourages learning low-rank weight matrices that exclusively depends on the optimization process of SGD with weight decay, regardless of the weight initialization, geometric properties of the data, or dimensionality of the data, which are largely irrelevant to the analysis. The assumption $\lim_{T\to\infty}(\|W_{T-1}^l\|/\|W_T^l\|) = 1$ generally occurs in practice and is validated in Appendix B. As a special case, it holds when $\|W_T^l\|$ converges to a non-zero value.

4 Experiments

In the previous section we have seen that one can approximate the learned weight matrices using matrices of bounded rank. Since the bound becomes smaller as we increase λ, μ or decrease B, we make the following prediction:

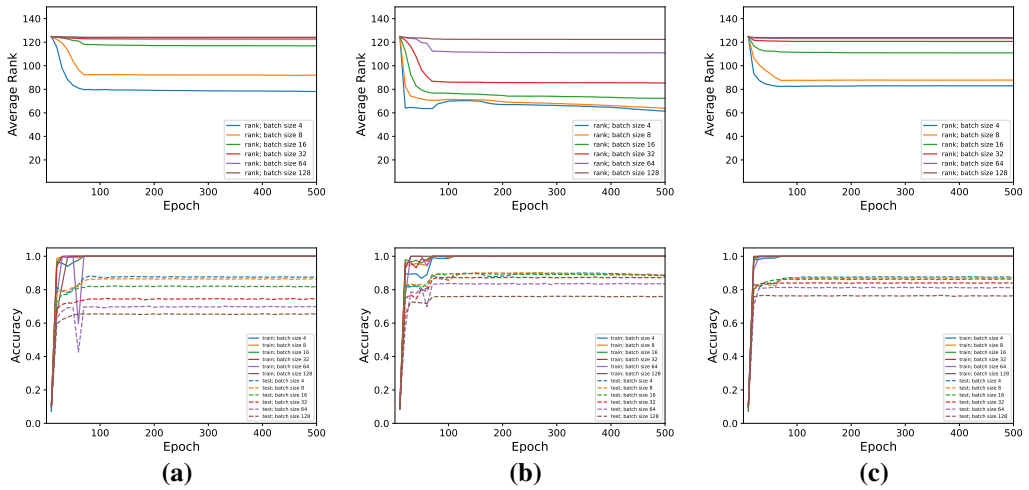

Figure 4: **Average ranks and accuracy rates of ResNet-18 trained on CIFAR10 when varying B.** In **(a)** we used $\mu = 1\text{e}{-3}$ and $\lambda = 6\text{e}{-3}$, in **(b)** we used $\mu = 5\text{e}{-3}$ and $\lambda = 6\text{e}{-3}$, and in **(c)** we used $\mu = 1\text{e}{-2}$ and $\lambda = 4\text{e}{-4}$. We used a threshold of $\epsilon = 1\text{e}{-3}$.

Prediction 4.1. *When training a neural network using SGD with weight decay, the effective rank of the learned weight matrices tends to decrease as the batch size decreases, or as the weight decay or learning rate increases.*

While the effective rank of a given matrix can be measured in various ways, in the experiments, we will focus on counting how many singular values of the normalized version of the matrix exceed a predefined threshold $\epsilon > 0$ (we use $\epsilon = 1\text{e}{-3}$ unless stated otherwise). In order to validate this prediction, we empirically study how batch size, weight decay, and learning rate affect the rank of matrices in deep networks. We conduct separate experiments where we vary one hyperparameter while keeping the others constant to isolate its effect on the average rank. Additional experiments with a variety of architectures (e.g., ViT, ResNet-18 and VGG-16), datasets (e.g., CIFAR10, MNIST, Fashion MNIST, SVHN), as well as visualizations of the singular values of the weight matrices are provided in Appendix B. The plots are best viewed when zooming into the pictures. Each of the runs was done using a single GPU for at most 60 hours on a computing cluster with several available GPU types (e.g., GeForce RTX 2080, Tesla V-100).

4.1 Setup

In each experiment we trained ResNet-18 [30] instances for classification using Cross-Entropy loss minimization using SGD with batch size B, initial learning rate μ, 0 momentum, and weight decay λ. The models were trained with a decreasing learning rate of 0.1 at epochs 60, 100, and 200, and the training was stopped after 500 epochs. During training, we applied random cropping, random horizontal flips, and random rotations (by $15k$ degrees for k uniformly sampled from $[24]$) and standardized the data.

To study the influence of different hyperparameters on the rank of the weight matrices, in each experiment, we trained the models while varying one hyperparameter at a time, while keeping other hyperparameters constant. After each epoch, we compute the average rank across the network's weight matrices and its train and test accuracy rates. For a convolutional layer we represent its kernel parameters as a matrix, whose rows are vectorized versions of its kernels. To estimate the rank of a given matrix M, we count how many of the singular values of $\frac{M}{\|M\|_2}$ are out of the range $[-\epsilon, \epsilon]$, where ϵ is a small tolerance value (we used $\epsilon = 1\text{e}{-3}$ by default).

4.2 Results

Validating prediction 4.1. As shown in Figs. 1-4, a smaller batch size or higher learning rate and weight decay leads to a smaller average rank across the network layers. Additionally, Fig. 3 shows that the effect of batch size on the ranks of the weight matrices is minimal when $\lambda = 0$, suggesting that weight decay is essential for imposing a noticeable low-rank bias on the weight matrices. These results align with prediction 4.1.

Low-rank bias and generalization. We investigated the relationship between low-rank bias and generalization by training ResNet-18 models on CIFAR10 with varying batch sizes, while keeping λ and μ constant. To provide a fair comparison, we selected λ and μ to ensure all models perfectly fit the training data. Our results, shown in Fig. 4, indicate that models trained with smaller batch sizes (and as a result with matrices of lower ranks) tend to have a better test performance. Based on these findings, we predict that when altering a certain hyperparameter, a neural network with a lower average rank will have better test performance than a network with the same architecture but higher rank matrices, assuming both networks perfectly fit the training data. For a similar experiment with VGG-16 [34] see Fig. 12 in Appendix B.

5 Conclusions

Mathematically characterizing the inductive biases of neural networks trained with SGD remains a significant open problem in the theory of deep learning [35]. In this work, we address one of the key inductive biases observed in empirical studies: the implicit minimization of the rank of learned weight matrices during training. Through our theoretical analysis of the training dynamics of regularized SGD, we identify a forgetting mechanism, where past updates are forgotten exponentially fast, resulting in learned weights that can be approximated by a mixture of recent training updates. This process leads to a rank minimization mechanism influenced by batch size, learning rate, and weight decay. Notably, this behavior appears largely independent of the geometry of the training data or its intrinsic dimensionality.

A promising direction for future work is to explore whether this theoretical framework can shed light on other empirical phenomena, such as emergent sparsity in neural networks [10], Neural Collapse in intermediate layers [36, 37], and Grokking [38]. Additionally, it would be valuable to investigate how other factors, such as momentum, affect the rank of the learned matrices and whether our findings can inspire new algorithms for compressing neural networks. Lastly, it would be interesting to study the relationship between this inductive bias and generalization, which seems plausible based on our empirical observations.

Acknowledgements

This work was supported by the Center for Brains, Minds and Machines (CBMM), funded by NSF STC award CCF - 1231216.

References

[1] Léon Bottou. Stochastic gradient learning in neural networks. In *Proceedings of Neuro-Nîmes 91*, Nimes, France, 1991. EC2.

[2] Chiyuan Zhang, Samy Bengio, Moritz Hardt, Benjamin Recht, and Oriol Vinyals. Understanding deep learning requires rethinking generalization. *CoRR*, abs/1611.03530, 2016.

[3] Stanislaw Jastrzebski, Zachary Kenton, Devansh Arpit, Nicolas Ballas, Asja Fischer, Yoshua Bengio, and Amos Storkey. Three factors influencing minima in sgd, 2017.

[4] Nitish Shirish Keskar, Dheevatsa Mudigere, Jorge Nocedal, Mikhail Smelyanskiy, and Ping Tak Peter Tang. On large-batch training for deep learning: Generalization gap and sharp minima. In *International Conference on Learning Representations (ICLR)*, 2017.

[5] Zhanxing Zhu, Jingfeng Wu, Bing Yu, Lei Wu, and Jinwen Ma. The anisotropic noise in stochastic gradient descent: Its behavior of escaping from sharp minima and regularization effects. In *Proceedings of the 36th International Conference on Machine Learning*, volume 139 of *Proceedings of Machine Learning Research*. PMLR, 2019.

[6] Elad Hoffer, Itay Hubara, and Daniel Soudry. Train longer, generalize better: closing the generalization gap in large batch training of neural networks. In I. Guyon, U. Von Luxburg, S. Bengio, H. Wallach, R. Fergus, S. Vishwanathan, and R. Garnett, editors, *Advances in Neural Information Processing Systems*, volume 30. Curran Associates, Inc., 2017.

[7] Yann LeCun, John Denker, and Sara Solla. Optimal brain damage. In D. Touretzky, editor, *Advances in Neural Information Processing Systems*, volume 2. Morgan-Kaufmann, 1989.

[8] B. Hassibi, D.G. Stork, and G.J. Wolff. Optimal brain surgeon and general network pruning. In *IEEE International Conference on Neural Networks*, pages 293–299 vol.1, 1993.

[9] Song Han, Jeff Pool, John Tran, and William J. Dally. Learning both weights and connections for efficient neural networks. NIPS'15, page 1135–1143, Cambridge, MA, USA, 2015. MIT Press.

[10] Jonathan Frankle and Michael Carbin. The lottery ticket hypothesis: Finding sparse, trainable neural networks. In *International Conference on Learning Representations*, 2019.

[11] Namhoon Lee, Thalaiyasingam Ajanthan, and Philip Torr. SNIP: SINGLE-SHOT NETWORK PRUNING BASED ON CONNECTION SENSITIVITY. In *International Conference on Learning Representations*, 2019.

[12] Mao Ye, Chengyue Gong, Lizhen Nie, Denny Zhou, Adam Klivans, and Qiang Liu. Good subnetworks provably exist: pruning via greedy forward selection. In *Proceedings of the 37th International Conference on Machine Learning*, ICML'20. JMLR.org, 2020.

[13] Cristian Buciluundefined, Rich Caruana, and Alexandru Niculescu-Mizil. Model compression. KDD '06, page 535–541, New York, NY, USA, 2006. Association for Computing Machinery.

[14] Geoffrey Hinton, Oriol Vinyals, and Jeff Dean. Distilling the knowledge in a neural network, 2015.

[15] Rafael Müller, Simon Kornblith, and Geoffrey E Hinton. When does label smoothing help? In H. Wallach, H. Larochelle, A. Beygelzimer, F. d'Alché-Buc, E. Fox, and R. Garnett, editors, *Advances in Neural Information Processing Systems*, volume 32. Curran Associates, Inc., 2019.

[16] Byeongho Heo, Minsik Lee, Sangdoo Yun, and Jin Young Choi. Knowledge transfer via distillation of activation boundaries formed by hidden neurons. AAAI'19/IAAI'19/EAAI'19. AAAI Press, 2019.

[17] Jian Xue, Jinyu Li, and Yifan Gong. Restructuring of deep neural network acoustic models with singular value decomposition. In *Interspeech*, 2013.

[18] Emily L Denton, Wojciech Zaremba, Joan Bruna, Yann LeCun, and Rob Fergus. Exploiting linear structure within convolutional networks for efficient evaluation. In Z. Ghahramani, M. Welling, C. Cortes, N. Lawrence, and K.Q. Weinberger, editors, *Advances in Neural Information Processing Systems*, volume 27. Curran Associates, Inc., 2014.

[19] Jose M. Alvarez and Mathieu Salzmann. Compression-aware training of deep networks. In *Proceedings of the 31st International Conference on Neural Information Processing Systems*, NIPS'17, page 856–867, Red Hook, NY, USA, 2017. Curran Associates Inc.

[20] Murad Tukan, Alaa Maalouf, Matan Weksler, and Dan Feldman. No fine-tuning, no cry: Robust svd for compressing deep networks. *Sensors*, 21(16), 2021.

[21] Xiyu Yu, Tongliang Liu, Xinchao Wang, and Dacheng Tao. On compressing deep models by low rank and sparse decomposition. In *2017 IEEE Conference on Computer Vision and Pattern Recognition (CVPR)*, pages 67–76, 2017.

[22] Meng Zhang, Fei Liu, and Dongpeng Weng. Speeding-up and compression convolutional neural networks by low-rank decomposition without fine-tuning. *J. Real-Time Image Process.*, 20(4), may 2023.

[23] Tolga Ergen and Mert Pilanci. Revealing the structure of deep neural networks via convex duality. *arXiv preprint arXiv:2002.09773*, 2020.

[24] Greg Ongie and Rebecca Willett. The role of linear layers in nonlinear interpolating networks, 2022.

[25] Nadav Timor, Gal Vardi, and Ohad Shamir. Implicit regularization towards rank minimization in relu networks. *CoRR*, abs/2201.12760, 2022.

[26] Ziwei Ji and Matus Telgarsky. Directional convergence and alignment in deep learning. *CoRR*, abs/2006.06657, 2020.

[27] Thien Le and Stefanie Jegelka. Training invariances and the low-rank phenomenon: beyond linear networks. In *International Conference on Learning Representations*, 2022.

[28] Tolga Ergen and Mert Pilanci. Revealing the structure of deep neural networks via convex duality. In Marina Meila and Tong Zhang, editors, *Proceedings of the 38th International Conference on Machine Learning*, volume 139 of *Proceedings of Machine Learning Research*, pages 3004–3014. PMLR, 18–24 Jul 2021.

[29] Sanjeev Arora, Nadav Cohen, Wei Hu, and Yuping Luo. Implicit regularization in deep matrix factorization. In *Proceedings of the 33rd International Conference on Neural Information Processing Systems*, Red Hook, NY, USA, 2019. Curran Associates Inc.

[30] Kaiming He, Xiangyu Zhang, Shaoqing Ren, and Jian Sun. Deep residual learning for image recognition. In *2016 IEEE Conference on Computer Vision and Pattern Recognition (CVPR)*, pages 770–778, 2016.

[31] Ashish Vaswani, Noam Shazeer, Niki Parmar, Jakob Uszkoreit, Llion Jones, Aidan N Gomez, Ł ukasz Kaiser, and Illia Polosukhin. Attention is all you need. In *Advances in Neural Information Processing Systems*, volume 30. Curran Associates, Inc., 2017.

[32] Y. Lecun, L. Bottou, Y. Bengio, and P. Haffner. Gradient-based learning applied to document recognition. *Proceedings of the IEEE*, 86(11):2278–2324, 1998.

[33] Shai Shalev-Shwartz and Shai Ben-David. *Understanding Machine Learning: From Theory to Algorithms*. Cambridge University Press, USA, 2014.

[34] Karen Simonyan and Andrew Zisserman. Very deep convolutional networks for large-scale image recognition. *CoRR*, abs/1409.1556, 2014.

[35] Behnam Neyshabur, Srinadh Bhojanapalli, David Mcallester, and Nati Srebro. Exploring generalization in deep learning. In I. Guyon, U. Von Luxburg, S. Bengio, H. Wallach, R. Fergus, S. Vishwanathan, and R. Garnett, editors, *Advances in Neural Information Processing Systems*, volume 30. Curran Associates, Inc., 2017.

[36] Vardan Papyan, X. Y. Han, and David L. Donoho. Prevalence of neural collapse during the terminal phase of deep learning training. *Proceedings of the National Academy of Sciences*, 117(40):24652–24663, 2020.

[37] Tomer Galanti, Liane Galanti, and Ido Ben-Shaul. Comparative generalization bounds for deep neural networks. *Transactions on Machine Learning Research*, 2023.

[38] Alethea Power, Yuri Burda, Harri Edwards, Igor Babuschkin, and Vedant Misra. Grokking: Generalization beyond overfitting on small algorithmic datasets, 2022.

[39] Alexey Dosovitskiy, Lucas Beyer, Alexander Kolesnikov, Dirk Weissenborn, Xiaohua Zhai, Thomas Unterthiner, Mostafa Dehghani, Matthias Minderer, Georg Heigold, Sylvain Gelly, et al. An image is worth 16x16 words: Transformers for image recognition at scale. *arXiv preprint arXiv:2010.11929*, 2020.

A Proofs

Lemma A.1. *Let ℓ be a differentiable loss function, and let f_W be a model as described in Sec. 2. For any weight matrix W^l in f_W and any sample $x \in \mathbb{R}^d$, the following inequality holds:*

$$\text{rank}\left(\nabla_{W^l}\ell(f_W(x))\right) \;\leq\; m_l,$$

where m_l is a constant depending on the structure of the layer l (defined in Eq. 2).

Proof. Let $u_j = u_j^l(x, W_{|l})$, and let $f_W(x)_r$ denote the r-th coordinate of $f_W(x)$. By applying the chain rule, we have the following identity for the gradient:

$$\nabla_{W^l}\ell(f_W(x)) = \sum_{r=1}^{q} \frac{\partial \ell(f_W(x))}{\partial f_W(x)_r} \cdot \frac{\partial f_W(x)_r}{\partial W^l}.$$

Next, observe that:

$$\frac{\partial f_W(x)_r}{\partial W^l} = \sum_{j=1}^{m_l} \frac{\partial f_W(x)_r}{\partial W^l u_j} \cdot \frac{\partial W^l u_j}{\partial W^l} = \sum_{j=1}^{m_l} \frac{\partial f_W(x)_r}{\partial W^l u_j} \cdot u_j^\top.$$

Substituting this into the previous expression, we get:

$$\nabla_{W^l}\ell(f_W(x)) = \sum_{r=1}^{q} \frac{\partial \ell(f_W(x))}{\partial f_W(x)_r} \cdot \sum_{j=1}^{m_l} \frac{\partial f_W(x)_r}{\partial W^l u_j} \cdot u_j^\top.$$

We can now simplify this expression:

$$\nabla_{W^l}\ell(f_W(x)) = \sum_{j=1}^{m_l} \left(\sum_{r=1}^{q} \frac{\partial \ell(f_W(x))}{\partial f_W(x)_r} \cdot \frac{\partial f_W(x)_r}{\partial W^l u_j} \right) u_j^\top.$$

This represents a sum of m_l outer products of vectors, implying that the resulting matrix has a rank of at most m_l. □

Lemma 3.2. *Let $\|\cdot\|$ be any matrix norm and ℓ any differentiable loss function. Consider a model f_W as described in Sec. 2 and W^l be a weight matrix within f_W. Suppose we train f_W using SGD with batch size $B \in [m]$, learning rate $\mu > 0$ and weight decay $\lambda > 0$, where m is the total number of training samples. Then, for any integer $T > n$, the following inequality holds:*

$$\min_{\bar{W}^l:\, \text{rank}(\bar{W}^l) \leq m_l B n} \left\| \frac{W_T^l}{\|W_T^l\|} - \bar{W}^l \right\| \;\leq\; (1 - 2\mu\lambda)^n \cdot \frac{\|W_{T-n}^l\|}{\|W_T^l\|}.$$

Proof. Let $\tilde{S}_t \subset S$ the mini-batch that was used by SGD at iteration t. We have

$$\begin{aligned} W_T^l \;&=\; W_{T-1}^l - \mu \nabla_{W^l} L_{\tilde{S}_{T-1}}(f_{W_{T-1}}) - 2\mu\lambda W_{T-1}^l \\ &=\; (1 - 2\mu\lambda) W_{T-1}^l - \mu \nabla_{W^l} L_{\tilde{S}_{T-1}}(f_{W_{T-1}}). \end{aligned}$$

Similarly, we can write

$$W_{T-1}^l \;=\; (1 - 2\mu\lambda) W_{T-2}^l - \mu \nabla_{W^l} L_{\tilde{S}_{T-2}}(f_{W_{T-2}}).$$

This gives us

$$W_T^l \;=\; (1 - 2\mu\lambda)^2 W_{T-2}^l - \mu \nabla_{W^l} L_{\tilde{S}_{T-1}}(f_{W_{T-1}}) - \mu(1 - 2\mu\lambda) \nabla_{W^l} L_{\tilde{S}_{T-2}}(f_{W_{T-2}}).$$

By recursively applying this process n times, we have

$$\begin{aligned} W_T^l \;&=\; (1 - 2\mu\lambda)^n W_{T-n}^l - \mu \sum_{j=1}^{n} (1 - 2\mu\lambda)^{j-1} \nabla_{W^l} L_{\tilde{S}_{T-j}}(f_{W_{T-j}}) \\ &=:\; (1 - 2\mu\lambda)^n W_{T-n}^l + U_{T,n}^l. \end{aligned}$$

We notice that,

$$\nabla_{W^l} L_{\tilde{S}_{T-j}}(f_{W_{T-j}}) \;=\; \tfrac{1}{B} \sum_{x_i \in \tilde{S}_{T-j}} \nabla_{W^l} \ell_i(f_{W_{T-j}}(x_i)).$$

According to Lem. A.1, we have $\text{rank}(\nabla_{W^l} \ell_i(f_{W_{T-j}}(x_i))) \;\leq\; m_l$. Therefore, $\text{rank}(\nabla_{W^l} L_{\tilde{S}_{T-j}}(f_{W_{T-j}})) \;\leq\; Bm_l$ since $\nabla_{W^l} L_{\tilde{S}_{T-j}}(f_{W_{T-j}})$ is an average of B matrices of rank at most m_l. In particular, $\text{rank}(U^l_{T,n}) \leq m_l Bn$ since $U^l_{T,n}$ is a sum of n matrices of rank at most $m_l B$. Therefore, we obtain that

$$\min_{\bar{W}^l:\, \text{rank}(\bar{W}^l) \leq m_l Bn} \left\| W^l_T - \bar{W}^l \right\| \;\leq\; \left\| W^l_T - U^l_{T,n} \right\| \;=\; (1-2\mu\lambda)^n \|W^l_{T-n}\|.$$

Finally, by dividing both sides by $\|W^l_T\|$ we obtain the desired inequality. □

Theorem 3.3. *Let $\|\cdot\|$ be any matrix norm and ℓ a differentiable loss function and $\mu, \lambda > 0$ such that $\mu\lambda < 0.5$, $B \in [m]$, and $\epsilon > 0$. Consider a model f_W as described in Sec. 2 and W^l be a weight matrix within f_W. Suppose we train f_W using SGD with batch size $B \in [m]$, learning rate $\mu > 0$ and weight decay $\lambda > 0$, where m is the total number of training samples. Assume that $\lim_{T\to\infty} (\|W^l_{T-1}\| / \|W^l_T\|) = 1$. Then, for sufficiently large T,*

$$\min_{\bar{W}^i:\, \text{rank}(\bar{W}^i) \leq \frac{m_l B \log(2/\epsilon)}{2\mu\lambda}} \left\| \frac{W^l_T}{\|W^l_T\|} - \bar{W}^i \right\| \;\leq\; \epsilon.$$

Proof. We pick $n = \lceil \frac{\log(\epsilon/2)}{\log(1-2\mu\lambda)} \rceil$. Since n is independent of T, we have

$$\lim_{T\to\infty} \frac{\|W^l_{T-n}\|}{\|W^l_T\|} = \lim_{T\to\infty} \prod_{j=1}^{n} \frac{\|W^l_{T-j}\|}{\|W^l_{T-j+1}\|} = \prod_{j=1}^{n} \lim_{T\to\infty} \frac{\|W^l_{T-i}\|}{\|W^l_{T-i+1}\|} = 1.$$

Then, for any sufficiently large T, we have $\frac{\|W^l_{T-n}\|}{\|W^l_T\|} \leq 2$.

We notice that for the selected T, we have $(1-\mu\lambda)^n \leq \epsilon/2$. Hence, for any large T, we have,

$$(1-\mu\lambda)^n \frac{\|W^l_{T-n}\|}{\|W^l_T\|} \leq \epsilon$$

Furthermore, since $\mu\lambda < 0.5$, we also have $n \leq \frac{\log(2/\epsilon)}{2\mu\lambda}$ and $m_l Bn \leq \frac{m_l B \log(2/\epsilon)}{2\mu\lambda}$. Therefore, by Lem. 3.2, we have the desired inequality. □

B Additional Experiments

We conducted additional experiments with various learning settings, including training on different datasets and using different architectures, to provide additional evidence for the bias of SGD with weight decay toward rank minimization. The experimental setup and results are described below.

B.1 Experimental Details

Architectures. We consider five types of network architectures. **(i)** The first architecture is a multi-layer perceptron (MLP), denoted as MLP-BN-L-H, which comprises L hidden layers, each containing a fully-connected layer with width H, followed by batch normalization and ReLU activations. This architecture ends with a fully-connected output layer. **(ii)** The second architecture, referred to as RES-BN-L-H, consists of a linear layer with width H, followed by L residual blocks, and ending with a fully-connected layer. Each block performs a computation of the form $z + \sigma(n_2(W_2\sigma(n_1(W_1 z))))$, where $W_1, W_2 \in \mathbb{R}^{H\times H}$, n_1, n_2 are batch normalization layers, and σ is the ReLU function. **(iii)** The third architecture is the convolutional network (VGG-16) proposed by [34], with dropout replaced by batch normalization layers to improve training performance, and a single fully-connected layer at the end. **(iv)** The fourth architecture is the residual network (ResNet-18) proposed in [30]. **(v)** The fifth architecture is a small visual transformer (ViT) [39]. We used a standard ViT that splits the input images into patches of size 4×4, and includes 8 self-attention heads, each composed of

6 self-attention layers. The self-attention layers are followed by two fully-connected layers with a dropout probability of 0.1, and a GELU activation in between them.

Training and evaluation. We trained each model for classification using Cross-Entropy loss minimization between its logits and the one-hot encodings of the labels. The training was carried out by SGD with batch size B, initial learning rate μ, and weight decay λ. The MLP-BN-L-H, RES-BN-L-H, ResNet-18, and VGG-16 models were trained with a decreasing learning rate of 0.1 at epochs 60, 100, and 200, and the training was stopped after 500 epochs. The ViT models were trained using SGD with a learning rate that was decreased by a factor of 0.2 at epochs 60 and 100 and training was stopped after 200 epochs. During training, we applied random cropping, random horizontal flips, and random rotations (by $15k$ degrees for k uniformly sampled from $[24]$) and standardized the data.

B.2 Results

Training with different architectures. In the main text, we validated our predictions using the ResNet-18 architecture. For a more comprehensive analysis, we conducted similar experiments with additional architectures. Similar to the results in the main text, Figs. 5-13 show that, as we increase weight decay or learning rate or decrease batch size, the effective rank of the learned weight matrices tends to decrease. Additionally, when $\lambda = 0$, the influence of batch size or learning rate on the rank of the weight matrices is minimal, as seen in Figs. 5, 6, and 10.

Training with momentum. To ensure that our observations are applicable beyond just SGD with weight decay, we conducted an experiment to test whether they also hold for SGD with both weight decay and momentum. As shown in Fig. 5, our predictions regarding the regularization effects of hyperparameters remain consistent, even when momentum is included in the training process.

Training on different datasets. In Fig. 13, we trained ResNet-18 instances on the MNIST and SVHN datasets, varying the learning rate while keeping the batch size ($B = 16$) and weight decay ($\lambda = 5\text{e}{-4}$) constant. The observed behavior, previously noted for CIFAR-10, is also replicated for these different datasets.

Verifying that $\lim_{T\to\infty}(\|W_{T-1}^l\|/\|W_T^l\|) = 1$. In Thm. 3.3 (main text) we made the assumption that $\lim_{T\to\infty}(\|W_{T-1}^l\|/\|W_T^l\|) = 1$. In order to validate this assumption, we trained various models and monitored the ratio between the norms of each layer at consecutive epochs. In each plot at Figs. 14-15 we report the ratios across different layers for a neural network with a certain learning rate. As can be seen, the ratios consistently converge to 1 during training.

Singular values. In our previous experiments, we measured the average rank of the weight matrices across different layers. To further investigate the rank of the learned weight matrices, we created visualizations displaying the singular values of the weight matrices for each layer as a function of batch size.

For instance, in Figs. 16-17 we plotted the singular values of various layers for models that were trained in the setting of Fig. 4(b) (main text) and Fig. 12(c). Our results indicate that as a general tendency the singular values of each layer can be partitioned into two distinct groups: "small" singular values and "large" singular values (see the intersection point of all curves in the plots). Interestingly, the number of "small" singular values and "large" singular values is generally independent of the batch size. Moreover, "large" singular values decrease with the batch size and the "small" singular values increase with the batch size. This behavior provides additional evidence that when training with smaller batch sizes, the matrices have fewer large singular values compared to training with larger batch sizes.

Comparing our bound with the averaged rank. As mentioned in the main text, our bound $m_l B \log(2/\epsilon)/(2\mu\lambda)$ is generally loose, but not trivial, as it scales as $\mathcal{O}(1)$ relative to the actual dimensions of the weight matrices. To demonstrate that our bound is non-trivial for wide neural networks, we trained an MLP-BN-2-10000 (see Appendix B.1 for details) on CIFAR10 using $B = 6$, $\mu = 0.1$, and $\lambda = 8\text{e}{-3}$. As shown in Figure 18, the network is able to train (achieves a non-trivial training accuracy), and at the same time, the bound is strictly smaller than the width of 10000 for any $\epsilon \geq 0.3$.

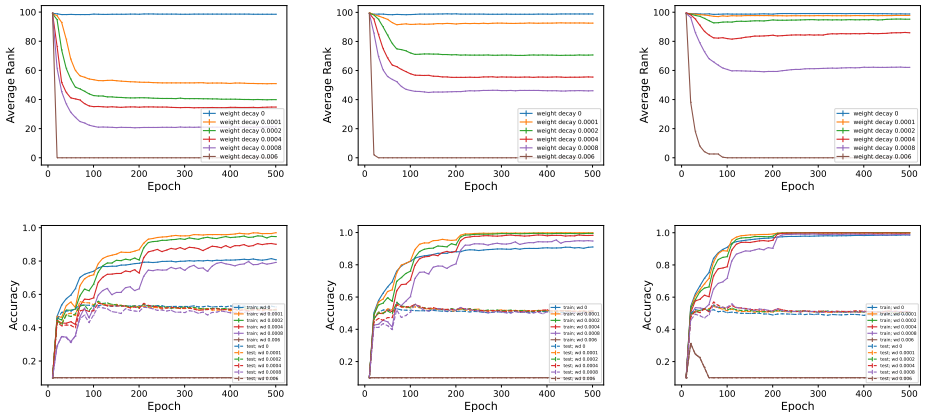

$B = 32$ $B = 64$ $B = 128$

Figure 5: **Average rank of MLP-BN-10-100 trained on CIFAR10 when varying λ.** In this experiment, $\mu = 0.1$, momentum 0.9 and $\epsilon = 1\text{e}{-3}$.

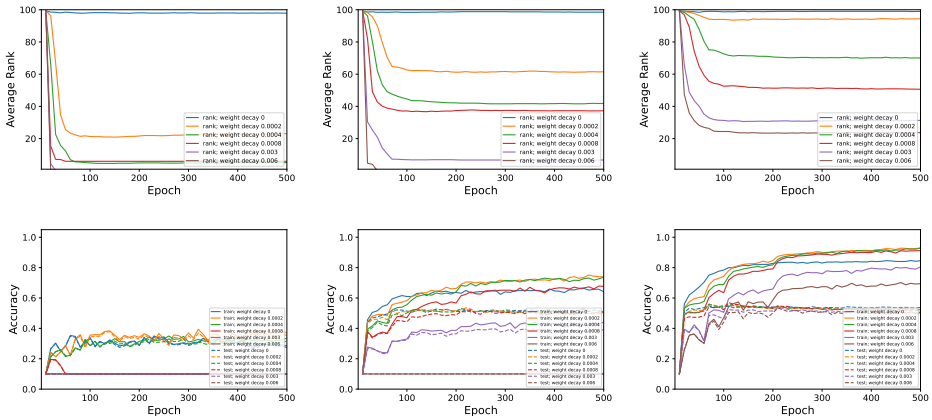

$B = 4$ $B = 8$ $B = 16$

Figure 6: **Average ranks and accuracy rates of MLP-BN-10-100 trained on CIFAR10 when varying λ.** In this experiment, $\mu = 0.1$ and $\epsilon = 1\text{e}{-3}$.

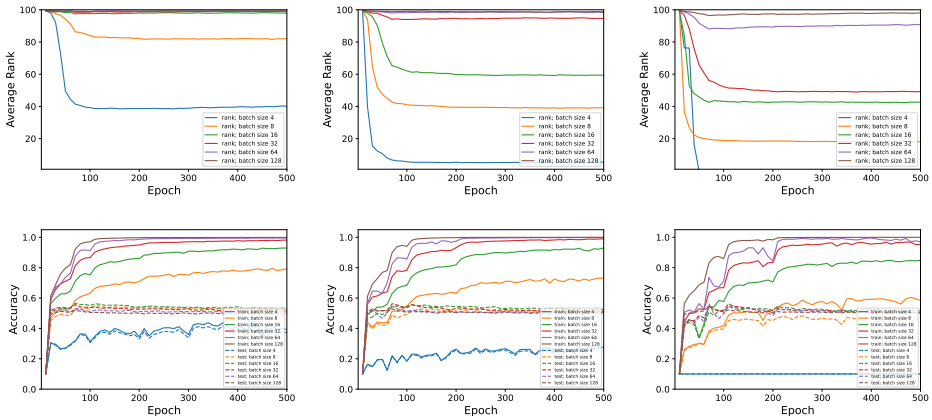

$\mu = 0.03$ $\mu = 0.1$ $\mu = 0.3$

Figure 7: **Average ranks and accuracy rates of MLP-BN-10-100 trained on CIFAR10 when varying B.** In this experiment, $\lambda = 5\text{e}{-4}$ and $\epsilon = 1\text{e}{-3}$.

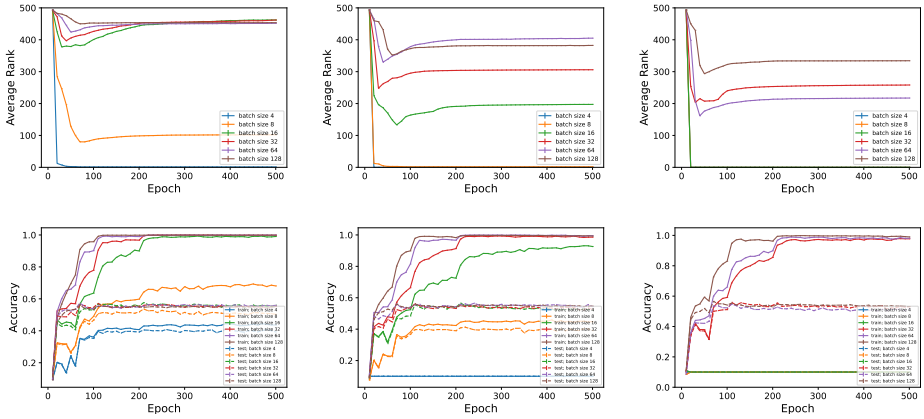

$\mu = 0.025$ $\mu = 0.05$ $\mu = 0.1$

Figure 8: **Average rank of RES-BN-5-500 trained on CIFAR10 when varying B.** In this experiment, $\lambda = 5\text{e}{-4}$ and $\epsilon = 1\text{e}{-3}$.

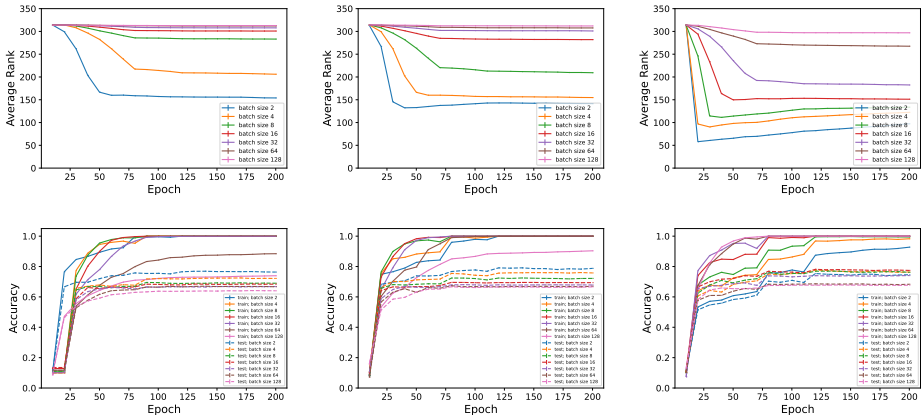

$\mu = 0.004$ $\mu = 0.008$ $\mu = 0.04$

Figure 9: **Average ranks and accuracy rates of ViT trained on CIFAR10 when varying B.** In this experiment, $\lambda = 5\text{e}{-4}$ and $\epsilon = 1\text{e}{-3}$.

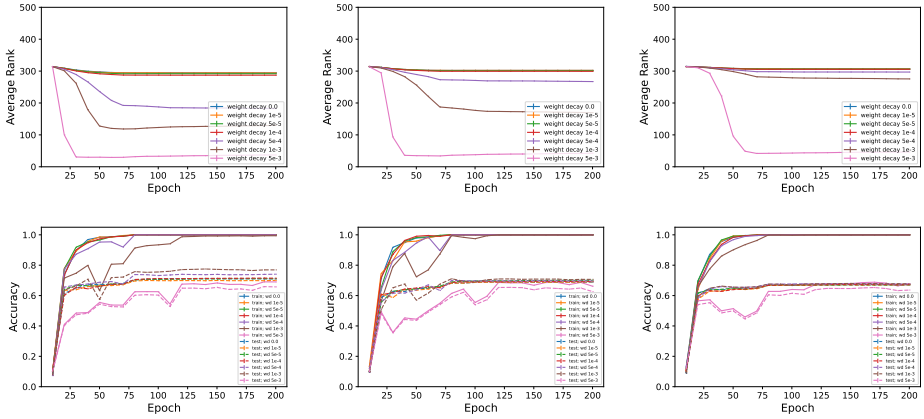

$B = 32$ $B = 64$ $B = 128$

Figure 10: **Average ranks and accuracy rates of ViT trained on CIFAR10 when varying λ.** In this experiment, $\mu = 4\text{e}{-2}$ and $\epsilon = 1\text{e}{-3}$.

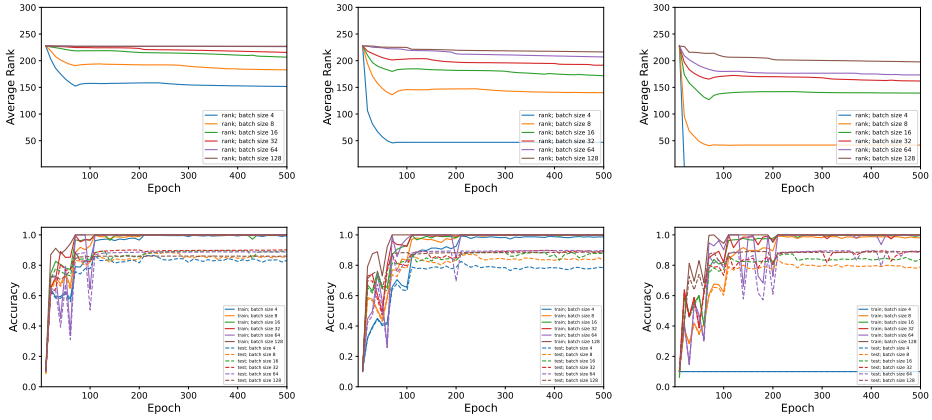

$\mu = 0.5$ $\mu = 1.0$ $\mu = 2.0$

Figure 11: **Average ranks and accuracy rates of ResNet-18 trained on CIFAR10 when varying B.** In this experiment, $\lambda = 5\text{e}{-4}$ and $\epsilon = 1\text{e}{-3}$.

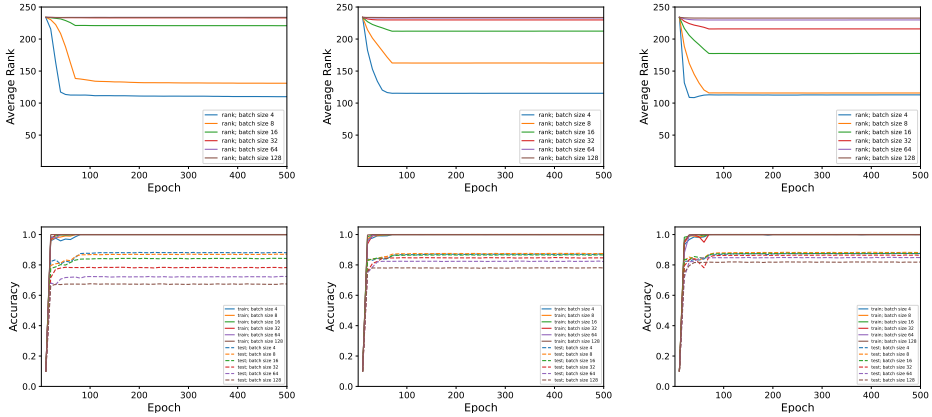

(a) $\mu = 1\text{e}{-3}, \lambda = 6\text{e}{-3}$ **(b)** $\mu = 5\text{e}{-3}, \lambda = 5\text{e}{-4}$ **(c)** $\mu = 1\text{e}{-2}, \lambda = 4\text{e}{-4}$

Figure 12: **Average ranks and accuracy rates of VGG-16 trained on CIFAR10 when varying B.** We used a threshold of $\epsilon = 1\text{e}{-3}$.

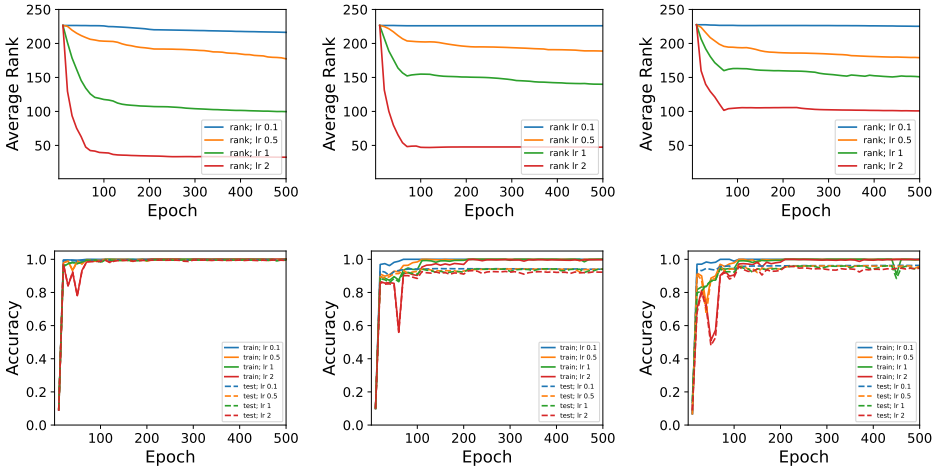

MNIST Fashion MNIST SVHN

Figure 13: **Average ranks and accuracy rates of ResNet-18 trained on MNIST, Fashion MNIST, and SVHN when varying μ.** In this experiment, $B = 16$, $\lambda = 5\text{e}{-4}$ and $\epsilon = 1\text{e}{-3}$.

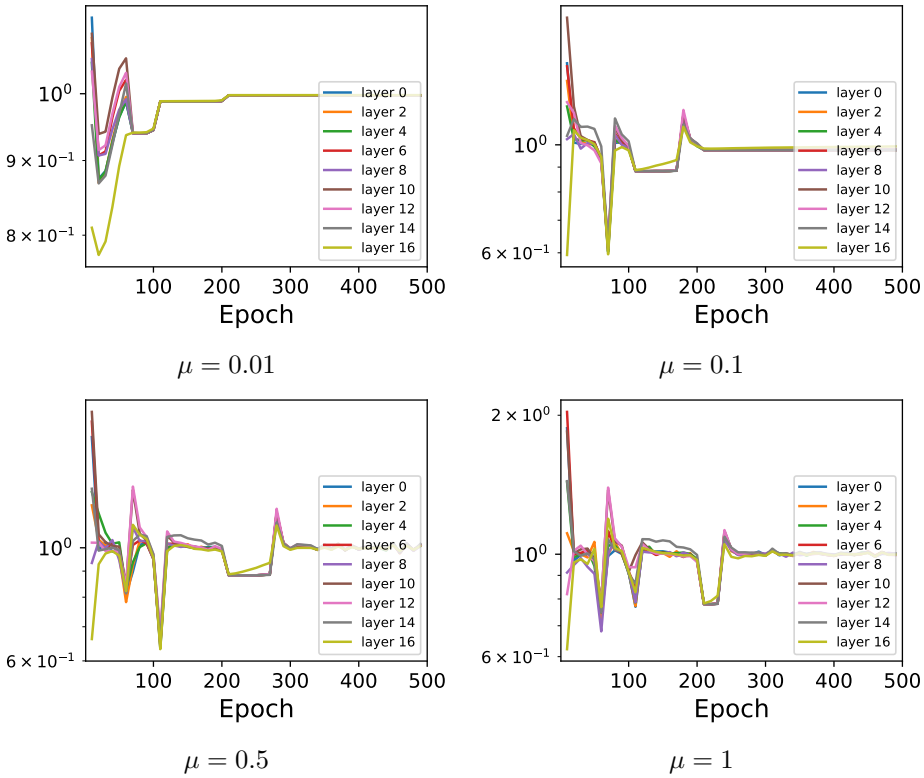

Figure 14: **Convergence of the weights for ResNet-18 trained on CIFAR10.** In this experiment, $B = 8$, $\lambda = 5\text{e}{-4}$ and $\epsilon = 0.01$ (see Fig. 2(mid) in the main text for the weight ranks and accuracy rates).

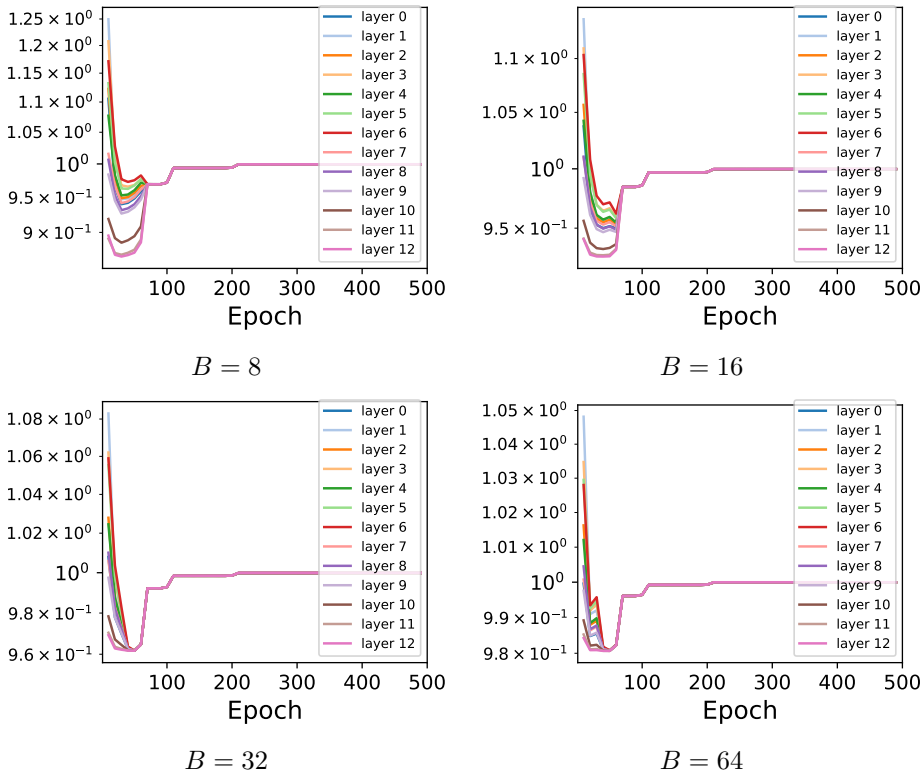

Figure 15: **Convergence of the weights for VGG-16 trained on CIFAR10.** In this experiment, $\mu = 5\text{e}{-3}$, $\lambda = 5\text{e}{-4}$ and $\epsilon = 0.01$ (see Fig. 12(b) for the weight ranks and accuracy rates).

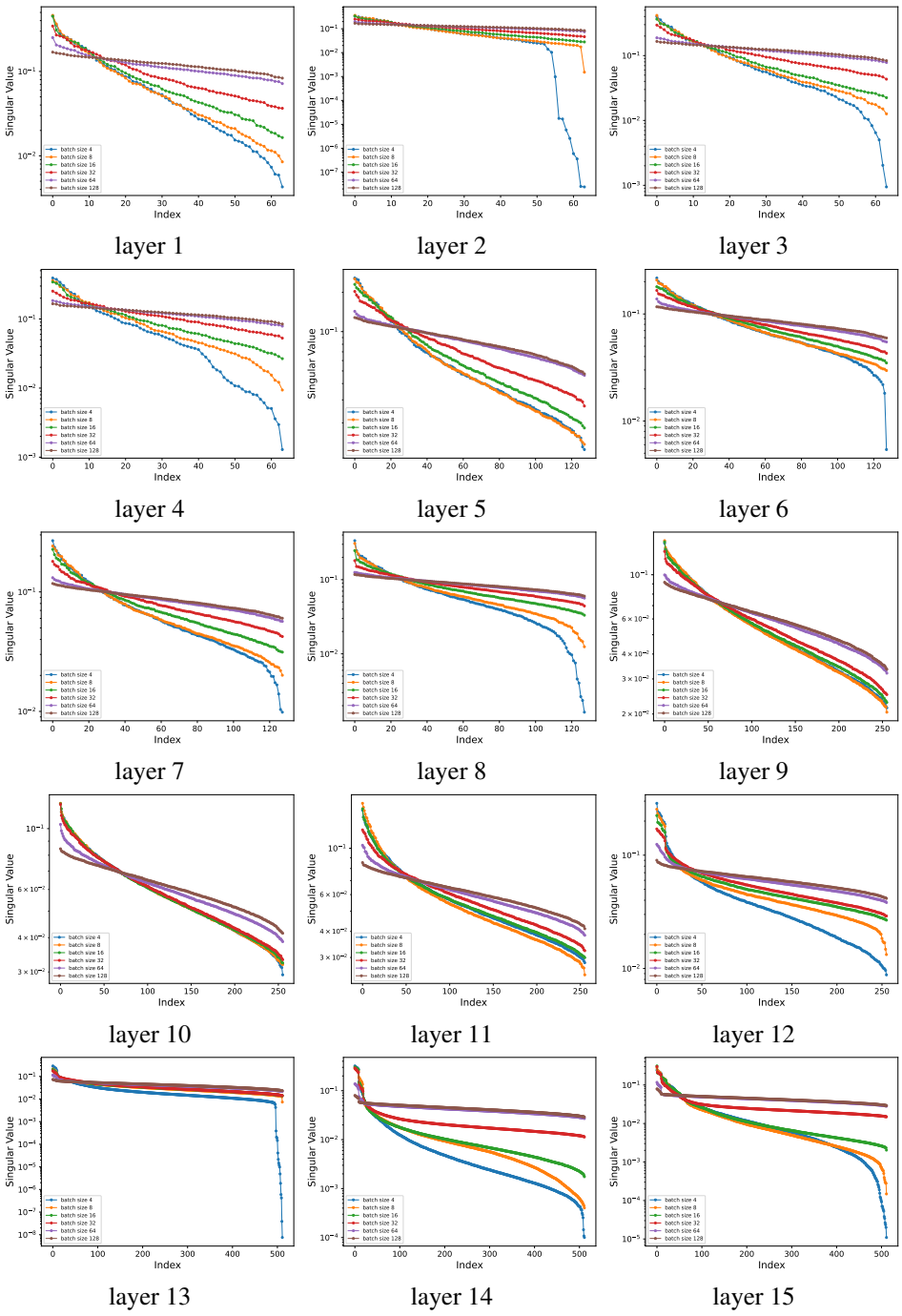

Figure 16: **Singular values of the weight matrices of ResNet-18 trained on CIFAR10 when varying B.** Each model was trained with $\mu = 5\text{e}{-3}$ and $\lambda = 6\text{e}{-3}$. Each plot reports the singular values of a given layer (see Fig. 4(b) in the main text for the averaged ranks and accuracy rates).

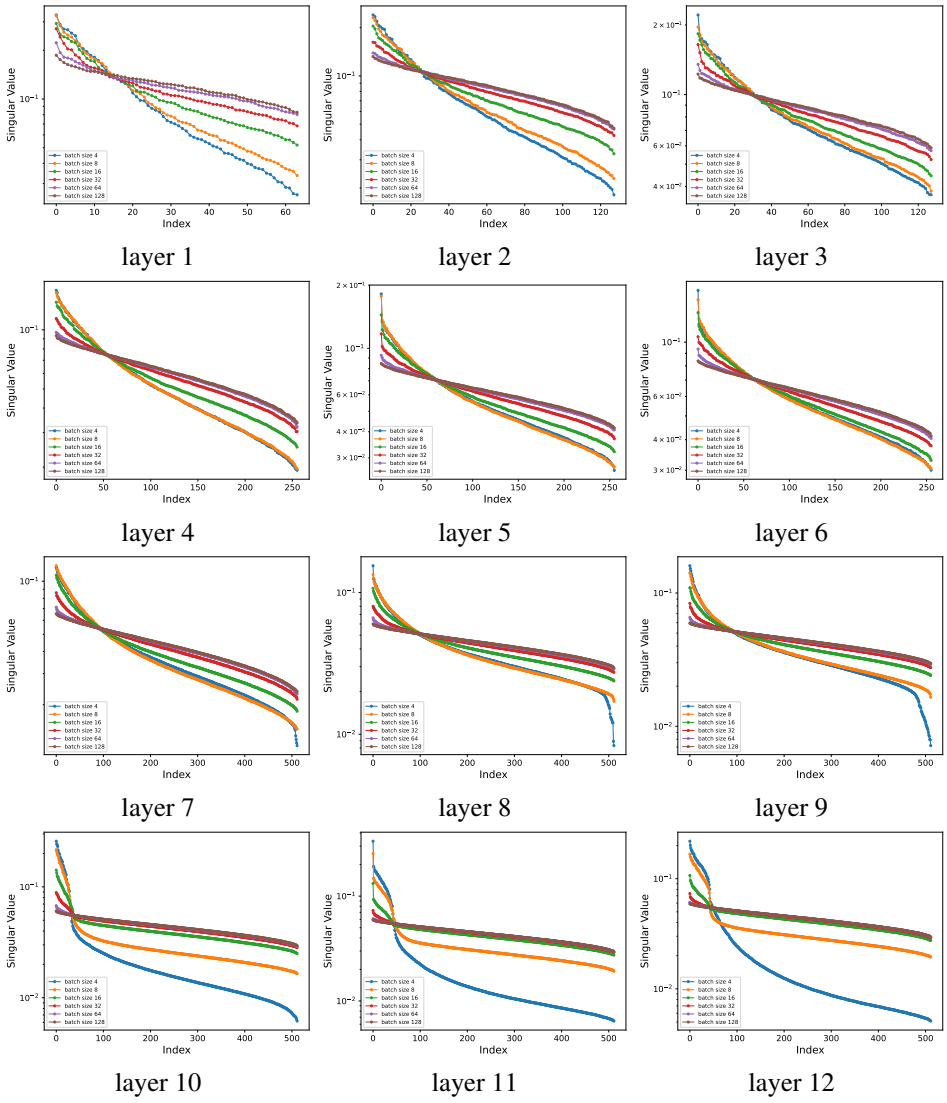

Figure 17: **Singular values of the weight matrices of VGG-16 trained on CIFAR10 when varying B.** Each model was trained with $\mu = 1\text{e}{-2}$ and $\lambda = 4\text{e}{-4}$. Each plot reports the singular values of a given layer (see Fig. 12(c) for the averaged ranks and accuracy rates).

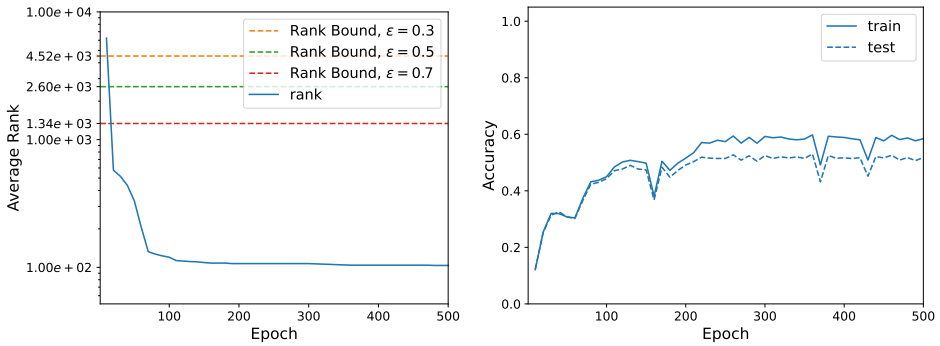

Figure 18: **Comparing our bound with the averaged rank.** We trained a MLP-BN-2-10000 on CIFAR10 with $B = 6$, $\mu = 0.1$, $\lambda = 8\text{e}{-3}$. We plot our bound for different choices of ϵ.